On design of differentially driven on-chip antennas with harmonic filtering for silicon integrated mm-wave and THz N-push oscillators

Janusz Grzyb[1], Yan Zhao[1,2], Richard Al Hadi[1], Ullrich Pfeiffer[1]
[1] IHCT, University of Wuppertal, Rainer-Gruenter-Str. 21, D-42119 Wuppertal, Germany
[2] now with the University of California at Los Angeles (UCLA), Los Angeles, CA 90095, USA

Abstract—**This paper reports on design of differentially driven lens-integrated on-chip ring antennas with harmonic filtering for both CMOS and SiGe HBT highly integrated mm-wave and THz N-push oscillators. Two state-of-the-art circuit/ antenna co-design examples of high-power sources are presented: at 288 GHz in 65nm CMOS technology and at 530 GHz in 0.13µm SiGe BiCMOS technology. The 530 GHz version is additionally extended into a 4x4 array with configurable radiation pattern diversity and capable of providing a total radiated power of up to 1mW.**

Index Terms— on-chip antenna, mm-wave, THz, CMOS, HBT SiGe, power source, active imaging, N-push oscillator.

I. Introduction

Over the last years tremendous progress has been made in the performance of highly integrated silicon room-temperature incoherent direct detectors [1-4]. Despite this progress, they still miss the sensitivity required for passive imaging and imagers need artificial illumination to provide the required image contrast. So far, expensive, high-power, focused illumination, single beam power sources are usually applied that limit the image quality due to its specular nature. However, active THz imaging might benefit from incoherent artificial sources to vary intensity, phase, frequency, and the direction of incoming light to reach the required lighting conditions; similar to visible light. For this purpose, truly low-cost, high-output power, and highly-integrated reconfigurable sources with high-quality on-chip antennas delivering optical quality of radiation are crucial for the success of active imaging systems [5]. However, in the 0.3-2 THz band, the output power of both electronic and photonic signal sources drops rapidly. Beyond device cut-off frequencies, the power cannot be amplified on-chip because transistors exhibit power loss. It can only be generated in the frequency translation process, e.g. by sub-harmonic mixers, harmonic multiplier chains, or harmonic N-push oscillators. The major drawbacks of the first two approaches are high chip area required and high DC power consumption; making them rather impractical for array arrangements [5,6]. Direct power generation by harmonic N-push oscillators, on the contrary, shows the potential of achieving dramatic reduction in both the chip real-estate (order of magnitude or more) and DC power consumption [7,8]. Despite these advantages, N-push oscillators also show some drawbacks manifesting themselves with an increased number of elements. In particular, the cancellation of unwanted harmonics is very sensitive to component mismatch and unwanted modes of operation need to be suppressed [9,10].

With this paper we would like to report on the design of silicon-integrated on-chip ring antennas intended to operate with N-push oscillator-based power sources. The considerations are based on two 3-push oscillator cores coupled differentially at the fundamental oscillation frequency. The first at 284-288 GHz is implemented in a bulk 65-nm CMOS process (*fmax* of 200 GHz) and delivers a radiated output power of -4.1 dBm [10]. The other operating at 519-536 GHz is realized in a 0.13µm SiGe BiCMOS technology with peak *ft/fmax* of 300/500 GHz, delivering the highest radiated power of -11.3dBm (85µW) ever reported for silicon technologies beyond 500 GHz [11]. In order to address the above-mentioned idea of source configurability, the latter was additionally implemented in a 4x4 array arrangement with programmable diversity and a total radiated power of up to 1mW.

II. Antenna-circuit co-design

Fig.1 shows the simplified schematics of both oscillator versions. In both cases, the ring antenna is differentially driven by two 3-push oscillators locked 180deg out-of-phase at the fundamental frequency in order to effectively generate radiation at the 3rd harmonic signal. The locking between two oscillator cores is realized by either capacitive coupling (530 GHz) or magnetic coupling (288GHz). Each core consists of 3 Colpitts or 3 ring oscillators with common push outputs through the base inductors or drain inductors, respectively. Differential topologies are of great interest because they can deliver higher output power to a single differential antenna; thus, resulting in considerable chip real-estate savings. The ideal circuit provides only a 3rd-harmonic differential output. However, due to the unavoidable mismatch in the circuit, different combinations of the fundamental and harmonic signals, both in common mode and differential mode, may leak to the antenna input. Due to the 180 deg out-of-phase locking between 2 oscillator cores, the following combination of parasitic harmonics will predominantly be present at the antenna port:

- 1st in differential mode (around 100 GHz and 180 GHz)
- 2nd in common mode (around 200 GHz and 360 GHz)
- 4th in common mode (around 400 GHz and 720 GHz)

Because of the absence of a buffering circuit in-between at such high operating frequencies, a true antenna-circuit co-design should be applied. The antenna should suppress the power from parasitic harmonic signals leaking from the non-ideal oscillating unit and allow low mutual coupling if applied in dense source array arrangements to prevent parasitic locking

in-between different oscillators. Such harmonics may deteriorate the inherent radiation patterns or lead to parasitic down-conversion at the receiver side. Furthermore, the antenna should deliver appropriate input impedance to the oscillating unit at different harmonics for maximum oscillation swing.

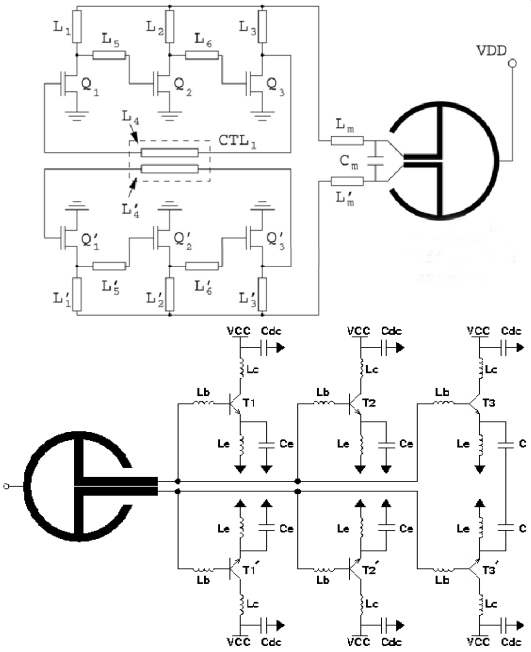

Fig. 1. Simplified schematics of the 3-push differential oscillators made of 2 mutually coupled single-ended 3-stage oscillator cores with differential ring antenna. Oscillator at 288 GHz with locking scheme by magnetic coupling (top); oscillator at 530 GHz with locking scheme by capacitive coupling (bottom).

III. Antenna design

A. Basic topology description

Along with the classical requirements on antenna performance related to the required operation bandwidth and radiation efficiency, efficient coupling to a quasi-optical system is of great interest. The latter, being a persistent problem for on-substrate antennas, has become one of the main motivations for the use of lens-coupled on-chip planar antennas [4,5,12]. A set of broadband on-chip wire-type linearly polarized ring antennas illuminating silicon lenses through the chip backside was developed to work with the considered harmonic oscillators. A metal-level antenna simulation model and the chip micrographs of two oscillators with antennas are shown in Figs. 2 and 3, respectively. The antennas span over the multi-layer BEOL metal stacks and include all dummy fillers to be compliant with the process design rules.

The main antenna part consists of 2 wire semi-rings connected along the center feed and is driven differentially from a harmonic source located aside (see Figs. 2 and 3). The center feed is non-uniformly tapered using stepwise approximation together with the appropriate ring width to provide the required impedance frequency characteristics. The proposed antenna layout promotes rotational symmetry of the radiated fields. All routing into the antenna center is along the H-plane (zero-field intensity) for radiation purity. This feature also allows circuit biasing through the antenna without any additional bandwidth limiting RF chokes ('Bias port' in Fig. 2). The antenna shows a simulated low cross-polarization level below -30 dB for differential signals, whereas for common-mode harmonics it can be considered as a monopole-like radiator with polarization orthogonal to that excited by differential signal. This interesting feature provides built-in test functionality for indirect measurements of the leakage level and the locking accuracy between 2 differentially coupled oscillator cores connected to the antenna RF port.

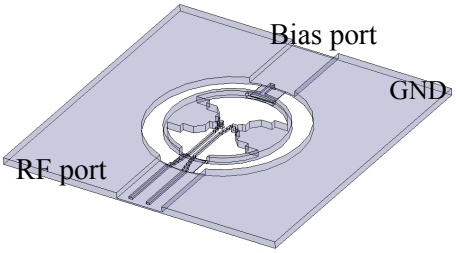

Fig. 2. Metal-level antenna geometry embedded within the back-end-of-the-line (BEOL) dielectric stack on a silicon chip.

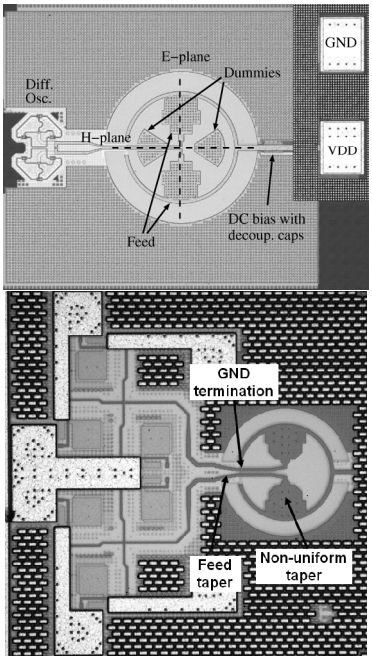

Fig. 3. Micrographs of the fabricated oscillator circuits with on-chip ring antennas. The 288 GHz version in 65nm CMOS (top); the 530 GHz version in 130nm SiGe (bottom). The antennas occupy 290µm x 290µm and 160µm x 160µm, respectively. The substrate thickness and silicon bulk resistivity are 185µm and 15Ω.cm, and 150µm and 50Ω.cm for the CMOS and SiGe process technologies, respectively.

Choosing a wire-type antenna with no direct proximity to GND planes is favorable for ohmic loss minimization [4]. Furthermore, it should be noted that substrate conductivity loss is of DC type while dielectric polarization and ohmic loss scale with frequency. In view of the miniature antenna size at the operation frequency and a chip thickness ranging from 150µm to 185µm, the applied bulk silicon substrate with a resistivity of 15 Ω.cm and 50 Ω.cm still allows to keep a high radiation efficiency (70-85% simulated into a semi-infinite silicon substrate with ideal lossless BEOL dielectric stack assumed).

The antenna was designed to minimize the radiated power from the major unwanted harmonics (see Sec. II for the list) by providing the highest possible reflection coefficient at its input, minimum conversion between common and differential modes, and lowering the antenna inherent radiation efficiency for parasitic spurs wherever possible.

B. Design details

A detailed design description will be given for the 530 GHz version. The same analysis can be applied for the 288 GHz version.

The center non-uniformly shaped part of the antenna plays a major role in defining the impedance bandwidth in differential operation regime (see Fig. 3). This altogether with the ring width and the ring diameter primarily define the frequency-dependent antenna impedance characteristics. The impedance bandwidth can be made very wide as in the considered case (matched to 100 Ω), where a -20-dB operation bandwidth spans from 350 to 740 GHz (see Fig. 6). Such an operation bandwidth can be viewed as suboptimal in terms of the higher-order harmonic attenuation but their power content at frequencies close to THz is negligible. The higher-end of the operation bandwidth can easily be reduced by redesign of the non-uniformly shaped part of the feed line in the ring center.

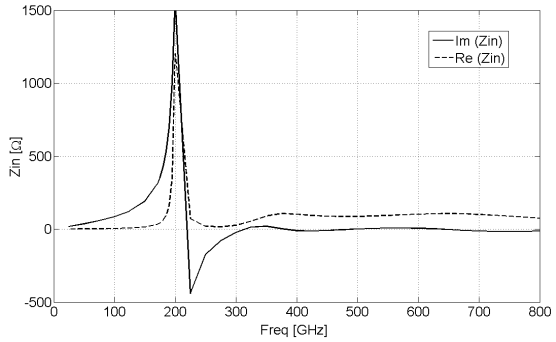

Fig. 4. Simulated input impedance for differential exciations at RF port (see Fig. 2) of the 530 GHz antenna.

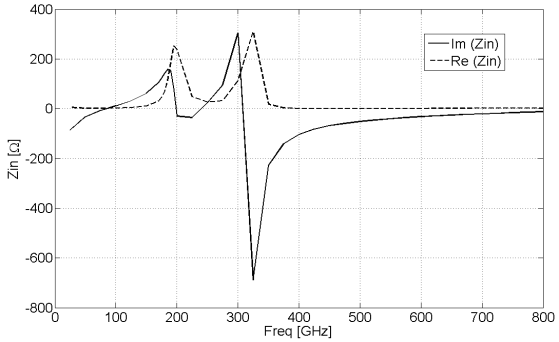

Fig. 5. Simulated input impedance for comon-mode exciations at RF port (see Fig. 2) of the 530 GHz antenna.

Between the oscillator core and the antenna ring, the feed line is tapered, bringing two lines close to each other. The purpose of this action is twofold. For differential operation, it rebuilds the field distribution along the feed line from two separate microstrip lines to a true differential system with minimized influence of the underlying GND plane (see Fig. 3). This provides a seamless well-matched transition down to the ring center with low differential-to-common mode conversion and minimizes parasitic radiation from that part of the feed line where the GND plane is no longer present (inside the ring). For common-mode operation, the tapered line changes its impedance profile along the line and effectively increases the reflection coefficient at the antenna RF port.

The ring-to-GND spacing additionally influences the antenna radiation pattern in differential operation mode and antenna characteristics for the common mode excitations.

It should also be noted that the GND plane underneath the feed line needs to be broken before reaching the ring center. The right location for this action plays a crucial role for the antenna behavior in the common-mode operation regime. It was found that the optimum location is the antenna ring, wherein the ring can locally take the role of the abruptly broken GND (see Fig. 3). For this position, the reflection coefficient at RF port and leakage to DC feed port for common-mode spurs are optimized (maximum reflection and minimum leakage) in the broad frequency range; specifically for the higher-order harmonics.

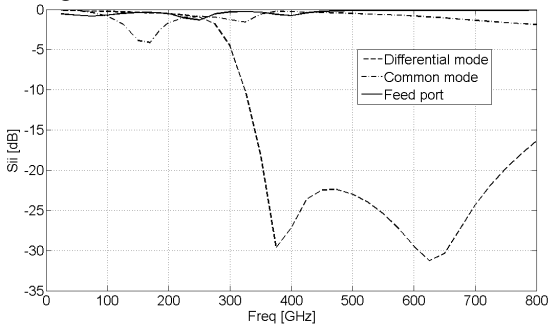

Fig. 6. Simulated reflection coefficients at the 530 GHz antenna ports. For RF port (see Fig. 2), both differential and common-mode excitations are considered.

The antenna input impedance for both differential and common-mode excitations is given in Figs. 4 and 5. The antenna provides almost constant 100 Ω differential impedance from around 350 GHz, whereas for the fundamental oscillation frequency (around 180 GHz) it presents a very high and reactive impedance; thus, guarantying almost perfect reflection. For the common-mode excitations, the antenna impedance behaves similar to a capacitive termination starting from around 330 GHz; thus, delivering a very high reflection coefficient for the 2nd-order harmonics. For the 1st–order common-mode harmonic signal, it becomes highly inductive and helps to quench the parasitic common-mode oscillation [9] at each of 2 differentially locked oscillator cores.

The antenna reflection coefficients for both differential and common modes at RF port are given in Fig. 6. The reflection coefficient for DC feed port is also presented.

The simulated mode conversion between common and differential modes at the RF port and the transmission from the RF port to the DC feed port for both differential and common mode excitations are gathered in Fig. 7. The differential RF-to-DC port transmission is inherently close to zero because of the AC ground present at the DC feed point. The common-mode transfer function, on the contrary, is strongly dependent on the antenna geometry and obviously will increase with the frequency decrease. The proper GND termination (on the ring),

as previously discussed, is here crucial to minimize it. For the same reason, the DC port should also be terminated with appropriately low impedance.

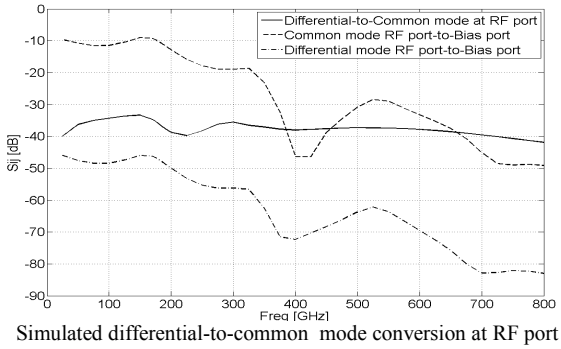

Fig. 7. Simulated differential-to-common mode conversion at RF port of the 530GHz antenna and RF-to-DC port leakage for both differential and common-mode excitations at RF port.

The corresponding simulated power radiated from the antenna for different excitation types at both antenna ports (RF and DC) is also given in Fig. 8.

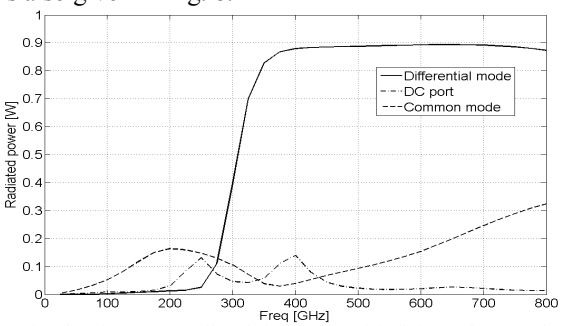

Fig. 8. Simulated power radiated into a semi-infinite substrate from the antenna for different excitation types at the antenna ports. All radiated powers are normalized to 1W incident power at the antenna inputs ports. 'DC port' stands for the power injected through the DC feed port on the antenna ring.

IV. Selected measured results

For test purposes, the single oscillator breakouts with on-chip antennas were mounted on electrically small diameter hyper-hemispherical silicon lenses with an extension length close to the elliptical position [13]. A 3-mm and 4-mm diameter lens was chosen for the 530 GHz and 288 GHz oscillator, respectively. The lenses were then attached to small PCBs (Fig. 9). The PCB surface surrounding the chip from the lens side was metalized to minimize back radiation from the source. A 4x4 oscillator array at 530 GHz with a close-packing layout was also manufactured (Fig.10) and combined with a 15-mm diameter lens. The EM simulations results of the complete 4x4 array show an inter-element coupling among all antennas below -35dB for the 350-800 GHz frequency range and practically negligible below 350 GHz. Each pixel in the array can be powered down independently such that arbitrary pattern configurations can be loaded serially and updated at runtime. The on-chip control circuitry is implemented in the CMOS process portion.

The output radiated power for each of the circuits was measured with a photo-acoustic absolute power meter (TK). To avoid the influence of heat generated on chip, the oscillators were chopped electronically by means of the on-chip digital circuitry. The power was also verified with an Erikson calorimeter (PM4). For pattern measurements in the far-field zone, the chip/lens/PCB assemblies were positioned in the pivotal point of a 2-axis computer-controlled rotational joint (see Fig. 11). A lens-coupled SiGe HBT direct detector [14] and an external harmonic down-conversion receiver from OML were applied on the receive side for 530 GHz and 288 GHz measurements, respectively.

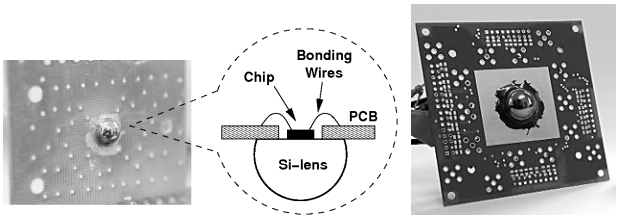

Fig. 9. Overall PCB assembly of the oscillator chips with silicon lenses. Assembly cross-section with a 3-mm diamater lens (left); 4x4 oscillator array at 530 GHz with a 15-mm diameter lens (right).

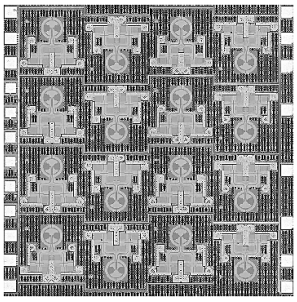

Fig. 10. Chip micrograph of the 4x4 source array at 530 GHz (2mm x 2.1mm)

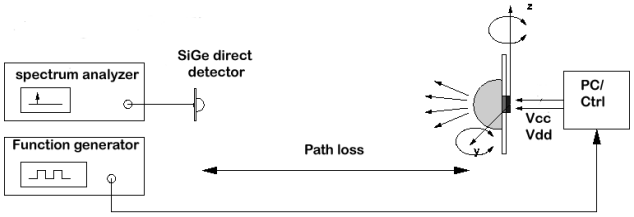

Fig. 11. Antenna pattern measurment setup.

For the 288 GHz CMOS source, an output power of -1.5 dBm and -4.1dBm was measured for the on-wafer breakout without antenna and for the 4-mm lens antenna-integrated version without matching cap, respectively. Under the assumption that both circuits exhibit a similar swing at the output, it results in an overall radiation efficiency of 55 %; being close to the simulated 65% for a 185µm thick Si substrate (15Ω.cm resistivity) on a 4-mm lens. The 530 GHz single oscillator with a 3-mm lens can deliver up to 85µW radiated output power, whereas the overall array radiating through a 15-mm lens provides a total radiated power of up to 1mW. The radiation efficiency cannot be de-embedded in this case because of the missing equipment for on-wafer measurements beyond 500 GHz. The simulated efficiency is around 80 % for a 3-mm lens assembly on a 150µm thick Si substrate (50Ω.cm resistivity). In this case, on-wafer measurements were only possible for the fundamental and 2nd harmonic leakage. The total leakage power measured with the PM4 was maximum 2µW. This power is further rejected below the free-space measurement setup sensitivity level due to the antenna harmonic attenuation.

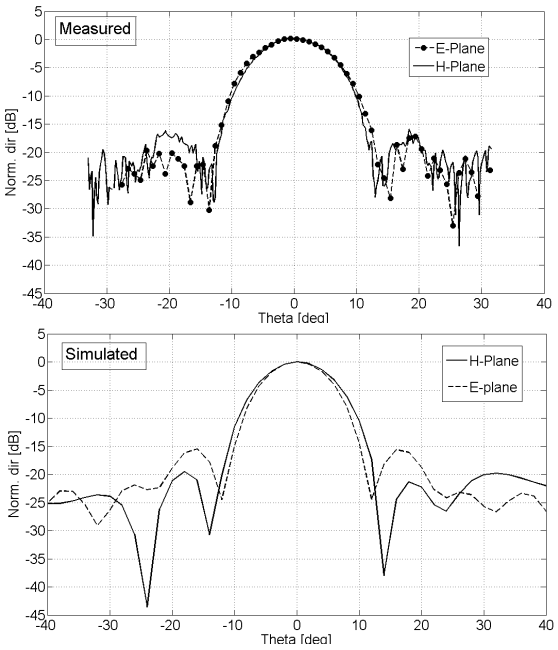

Fig. 12. Measured and simulated radiation patterns at 530 GHz for the oscillator combined with a 3-mm diameter lens without matching cap.

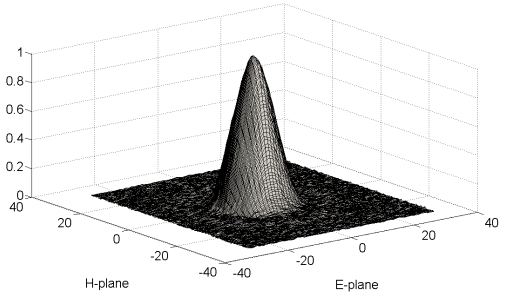

Fig. 13. 3-D view of the measured normalized radiation pattern at 530 GHz (linear scale).

Figs. 12 and 13 show the measured and simulated radiation patterns for the 530 GHz oscillator combined with a 3-mm lens, indicating good Gaussian shapes, rotational symmetry, and a low side-lobe level of around -20dB. Very good correspondence between simulations and measurements can be noticed.

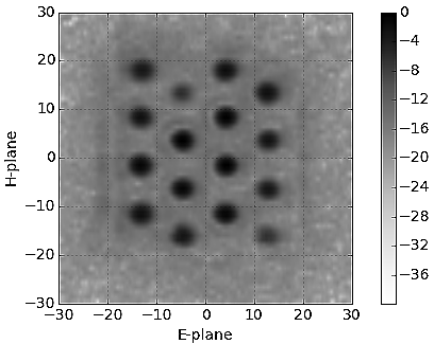

Fig. 14. Measured radiation pattern (top view) for the complete 4x4 array on a 15-mm diamater lens with all pixels activated.

An example of the radiation pattern for the complete 4x4 array on a 15-mm diameter lens with all pixels activated is shown in Fig. 14. The measured directivity derived from the FWHM of a single beam is 37dBi and all 16 beams cover a field of view of around ±15º.

V. Summary

Based on two state-of-the-art design examples of all-silicon integrated high-power sources at 288 GHz and 530 GHz with differential on-chip ring antennas, an innovative approach of generating and radiating power beyond device cut-off frequency was presented. Due to a true circuit/antenna co-design, the combined signal generation with frequency up-conversion and selective radiation with harmonic filtering of undesired spurious signals could be simultaneously achieved in a small silicon footprint. The presented ideas pave the way for implementation of a spatially distributed scene illumination with the capability of an arbitrary pattern generation updated at runtime.

References

[1] U. R. Pfeiffer, J. Grzyb, H. Sherry , A. Cathelin, A. Kaiser, "Toward Low-NEP Room-Temperature THz MOSFET Direct Detectors in CMOS Technology," IRMMW-THz 2013, pp.1-2, Sep. 2013.

[2] H. Sherry, J. Grzyb, Y. Zhao, R. Al Hadi, A. Cathelin, A. Kaiser, U. Pfeiffer, "A 1kPixel CMOS Camera Chip for 25fps Real-Time Terahertz Imaging Applications," ISSCC Dig. Tech. Papers, pp. 252-253, 2012.

[3] R. Al Hadi, H. Sherry, J. Grzyb, Y. Zhao, W. Forster, H. Keller, A. Cathelin, A. Kaiser, and U. Pfeiffer, "A 1 k-Pixel Video Camera for 0.7–1.1 Terahertz Imaging Applications in 65-nm CMOS," IEEE J. Solid-State Circuits, vol. 47, no. 12, pp. 2999–3012, Dec. 2012.

[4] J. Grzyb, H. Sherry, Y. Zhao, R. Al Hadi, A. Kaiser, A. Cathelin, and U. R. Pfeiffer, "Real-Time Video Rate Imaging with a 1k-pixel THz CMOS Focal-Plane Array", Proc. SPIE, vol. 8362, pp.1-12, April 2012.

[5] J. Grzyb, R. Al Hadi, Y. Zhao, U. Pfeiffer, "Toward Room-Temperature All-Silicon Integrated THz Active Imaging," EuCAP 2013, pp. 1740-1744, April. 2013, Sweden.

[6] E. Öjefors, J. Grzyb, B. Heinemann, B. Tillack, and U. R. Pfeiffer, "A 820 GHz SiGe Chipset for Terahertz Active Imaging Applications," IEEE International Solid-State Circuits Conference, pp. 224–225, 2011.

[7] O. Momeni, A. Afshari, "Hgh Power Terahertz and Millimeter-Wave Oscilator Design: A Systematic Approach," IEEE J. Solid-State Circuits, vol. 46, no. 3, pp. 583–597, March 2011.

[8] K. Sengupta, et.al, "A 0.28 THz Power Generation and Beam-Steering Array in CMOS Based on Distributed Active Radiators," IEEE J. Solid-State Circuits, vol. 47, no. 12, pp. 3013-3031, Dec. 2012.

[9] Y.-L. Tang, and H. Wang, "Triple-Push Oscillator Approach: Theory and Experiments," IEEE J. Solid-State Circuits, vol. 36, no. 10, pp. 1472-1479, Oct. 2001.

[10] J. Grzyb, Y. Zhao, U. Pfeiffer, "A 288-GHz Lens-Integrated Balanced Triple-Push Source in a 65-nm CMOS Technology," IEEE Solid-State Circuits Journal, vol. 48, no. 7, pp. 1751-1761, July 2013.

[11] U. Pfeiffer, Y. Zhao, J. Grzyb, R. Al Hadi, N. Sarmah, W. Forster, H. Rucker, B. Heinemann, "A 0.53THz Reconfigurable Source Array with up to 1mW Radiated Power for Terahertz Imaging Applications in 130nm SiGe BiCMOS," to appear in ISSCC 2014.

[12] J. Grzyb, R. Al Hadi, U. Pfeiffer, "Lens-Integrated On-Chip Antennas for THz Direct Detectors in SiGe HBT," AP-S 2013, July 2013, FL, USA.

[13] D. Filipovic, et al., "Double-Slot Antennas on Extended Hemispherical and Elliptical Silicon Dielectric Lenses," IEEE Trans. MTT, vol. 41, no. 10, pp. 1738–1749, Oct.1993.

[14] R. Al Hadi, J. Grzyb, B. Heinemann, U. Pfeiffer, "A Terahertz Detector Array in a SiGe HBT Technology," IEEE Solid-State Circuits Journal, vol. 48, no. 9, pp. 2002-2010, Sep. 2013.